J|A|C|S
A R T I C L E S

Spectroscopic and Computational Studies on the Adenosylcobalamin-Dependent Methylmalonyl-CoA Mutase: Evaluation of Enzymatic Contributions to Co–C Bond Activation in the Co³⁺ Ground State

Amanda J. Brooks,[†] Monica Vlasie,[‡] Ruma Banerjee,[‡] and Thomas C. Brunold*,[†]

Contribution from the Department of Chemistry, University of Wisconsin-Madison, Madison, Wisconsin 53706, and Department of Biochemistry, University of Nebraska, Lincoln, Nebraska 68588

Received October 17, 2003; E-mail: brunold@chem.wisc.edu

Abstract: Methylmalonyl-CoA mutase (MMCM) is an enzyme that utilizes the adenosylcobalamin (AdoCbl) cofactor to catalyze the rearrangement of methylmalonyl-CoA to succinyl-CoA. Despite many years of dedicated research, the mechanism by which MMCM and related AdoCbl-dependent enzymes accelerate the rate for homolytic cleavage of the cofactor's Co–C bond by ~12 orders of magnitude while avoiding potentially harmful side reactions remains one of the greatest subjects of debate among B_{12} researchers. In this study, we have employed electronic absorption (Abs) and magnetic circular dichroism (MCD) spectroscopic techniques to probe cofactor/enzyme active site interactions in the Co³⁺Cbl "ground" state for MMCM reconstituted with both the native cofactor AdoCbl and its derivative methylcobalamin (MeCbl). In both cases, Abs and MCD spectra of the free and enzyme-bound cofactor are very similar, indicating that replacement of the intramolecular base 5,6-dimethylbenzimidazole (DMB) by a histidine residue from the enzyme active site has insignificant effects on the cofactor's electronic properties. Likewise, spectral perturbations associated with substrate (analogue) binding to holo-MMCM are minor, arguing against substrate-induced enzymatic Co–C bond activation. As compared to the AdoCbl data, however, Abs and MCD spectral changes for the sterically less constrained MeCbl cofactor upon binding to MMCM and treatment of holoenzyme with substrate (analogues) are much more substantial. Analysis of these changes within the framework of time-dependent density functional theory calculations provides uniquely detailed insight into the structural distortions imposed on the cofactor as the enzyme progresses through the reaction cycle. Together, our results indicate that, although the enzyme may serve to activate the cofactor in its Co³⁺Cbl ground state to a small degree, the dominant contribution to the enzymatic Co–C bond activation presumably comes through stabilization of the Co²⁺Cbl/Ado• post-homolysis products.

1. Introduction

Heralded as one of the most complex cofactors found in nature, adenosylcobalamin (AdoCbl or coenzyme B_{12}) has been the focus of hundreds of publications since its discovery in 1958.[1-3] This cofactor and its closely related methylcobalamin (MeCbl) derivative possess unique structures (Figure 1), offering the only known instances of a stable organometallic bond in a biological system. Not surprisingly, the Co–C bond lies at the center of reactivity for the numerous enzymes that employ these extraordinary cofactors. Cobalamin cofactors consist of a low spin Co³⁺ ion that is equatorially ligated by four nitrogen atoms from a corrin macrocycle (Figure 1), which is similar to but more reduced than the ubiquitous porphyrin macrocycle. Axially,

the cobalt ion is coordinated on the "lower" face by a nitrogen from the intramolecular base 5,6-dimethylbenzimidazole (DMB) and on the "upper" face by either a CH_3 group (in MeCbl) or 5′-deoxyadenosyl (AdoCbl).[4] While enzymes utilizing AdoCbl catalyze radical-induced rearrangement reactions[5-7] or ribonucleotide reduction[8] via homolytic cleavage of the Co–C bond, MeCbl-dependent enzymes catalyze methyl-transfer reactions via heterolytic Co–C bond cleavage.[9,10] Understanding the mechanisms by which B_{12}-dependent enzymes activate the Co–C bond for homolysis or heterolysis continues to be an active area of intense research.

Methylmalonyl-CoA mutase (MMCM) is a member of a small class of AdoCbl-dependent enzymes that function as isomerases.[11] Other well-studied enzymes in this class include

† University of Wisconsin-Madison.
‡ University of Nebraska.
(1) Ludwig, M. L.; Matthews, R. G. *Annu. Rev. Biochem.* **1997**, *66*, 269–313.
(2) Marsh, E. N. G.; Drennan, C. L. *Curr. Opin. Chem. Biol.* **2001**, *5*, 499–505.
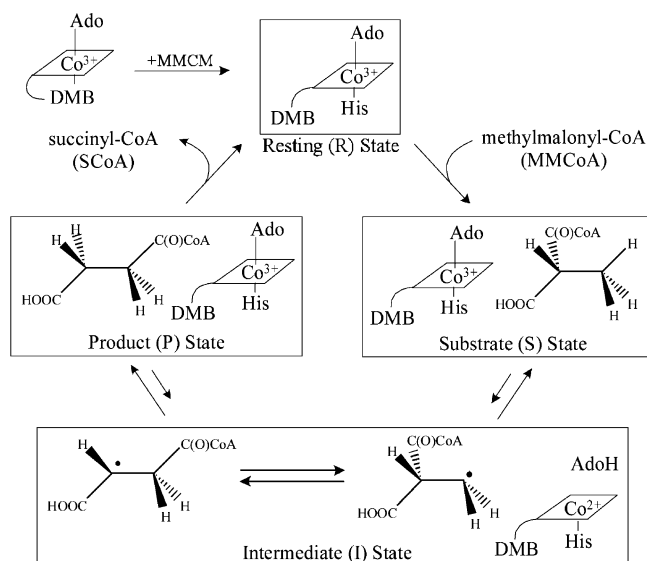(3) Banerjee, R., Ed. *Chemistry and Biochemistry of B₁₂*; Wiley-Interscience: New York, 1999.
(4) Lenhert, P. G.; Hodgkin, D. C. *Nature* **1961**, *192*, 937–938.
(5) Marsh, E. N. G. *Bioorg. Chem.* **2000**, *28*, 176–189.
(6) Frey, P. A.; Reed, G. H. *Arch. Biochem. Biophys.* **2000**, *382*, 6–14.
(7) Banerjee, R. *Biochemistry* **2001**, *40*, 6191–6198.
(8) Lawrence, C. C.; Stubbe, J. *Curr. Opin. Chem. Biol.* **1998**, *2*, 650–655.
(9) Matthews, R. G. In *Chemistry and Biochemistry of B₁₂*; Banerjee, R., Ed.; Wiley: New York, 1999; pp 681–706.
(10) Matthews, R. G. *Acc. Chem. Res.* **2001**, *34*, 681–689.
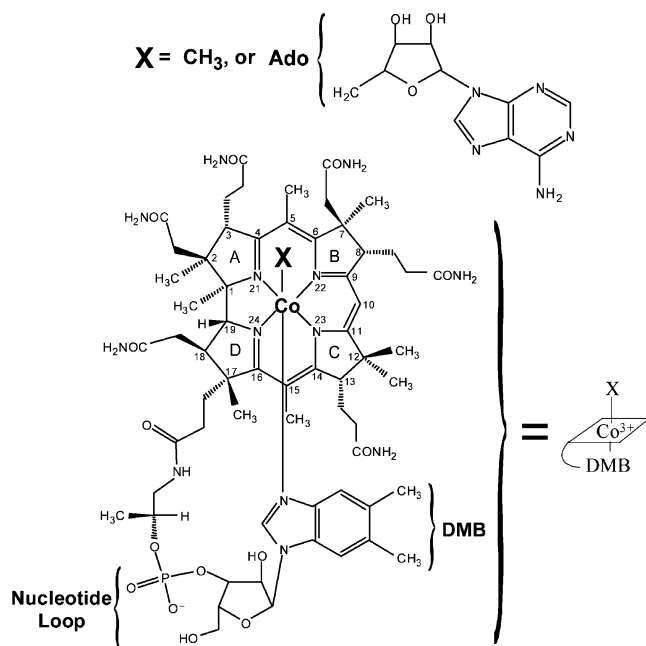
Figure 1. Chemical structure and numbering scheme for $Co^{3+}Cbls$, where **X** indicates the upper axial ligand.

Figure 2. Minimal mechanism for the homolytic cleavage and rearrangement reaction of MMCM, adapted from ref 20. Note that for MMCM reconstituted with MeCbl, a primed notation is used to designate the corresponding states (i.e., R′, S′, and P′ states).

glutamate mutase,[5] diol dehydratase,[12] and ethanolamine ammonia lyase;[13] however, MMCM is unique in being the only known isomerase to be present in both bacteria and mammals.[14] Common to all of these enzymes is the initial step in the enzymatic reaction, homolytic cleavage of the Co–C bond of the AdoCbl cofactor to generate Co^{2+}-cobalamin ($Co^{2+}Cbl$) and an organic radical centered on the 5′-carbon of the adenosyl moiety.[15] Enzymatic activation of this step is spectacular; for example, in the case of MMCM, the Co–C bond homolysis rate for the free AdoCbl cofactor (4×10^{-10} s^{-1} at 25 °C)[16] is raised by as much as 12 orders of magnitude.[17] Such activation entails a ~17 kcal/mol reduction in the Co–C bond dissociation enthalpy (BDE) from 31.4 ± 1.5 to ~14 kcal/mol.[18,19] The Ado• radical generated in this process then serves to abstract a hydrogen atom from the substrate in a protein-mediated carbon skeleton rearrangement. The minimal mechanism for the MMCM catalyzed rearrangement reaction of methylmalonyl-CoA to succinyl-CoA is presented in Figure 2.[20] Impairment of this mutase activity results in methylmalonic aciduria, an autosomal disorder that is often fatal in infants.[21]

The mechanism by which AdoCbl-dependent enzymes achieve the remarkable activation of the cofactor's Co–C bond while avoiding potentially harmful side reactions remains one of the greatest subjects of debate among B$_{12}$ researchers. Possible pathways by which the enzymes can overcome the large energetic barrier to Co–C bond homolysis include (i) destabilization of the $Co^{3+}Cbl$ ground state upon cofactor binding to MMCM (R state, Figure 2) and subsequent binding of substrate (analogue) to the holoenzyme (S and P states), (ii) stabilization of the $Co^{2+}Cbl$ and substrate/product radical intermediates, and (iii) a combination of (i) and (ii). Both steric and electronic factors contributing to this enzymatic Co–C bond activation have been explored through a large number of structural, spectroscopic, and computational studies.[18,20,22–27]

X-ray crystallographic studies on the bacterial *Propionibacterium shermanii* MMCM have shown that the enzyme crystallizes as a heterodimer of 80 and 69 kDa chains, with the larger subunit binding one molecule of AdoCbl.[28] These studies also confirmed earlier results from EPR spectroscopy[29] that, in the enzyme active site, the intramolecular DMB base of the cofactor is replaced by His^{610} as the lower axial ligand to the Co center. On the basis of crystallographic data at 2 Å resolution,[28] this ligand switch is accompanied by a slight flattening of the corrin macrocycle and possibly results in the formation of an unusually long Co–N$_{ax}$ bond (2.5 Å as compared to 2.2 Å for free AdoCbl[30]). However, subsequent EXAFS[24,31,32] and EPR[33] studies suggested that this Co–N$_{ax}$ bond lengthening might

(11) Banerjee, R. *Chem. Rev.* **2003**, *103*, 2083−2094.
(12) Toraya, T. *Chem. Rec.* **2002**, *2*, 352−366.
(13) Bandarian, V.; Reed, G. H. In *Chemistry and Biochemistry of B$_{12}$*; Banerjee, R., Ed.; Wiley: New York, 1999; pp 811−833.
(14) Ledley, F. D. *BioEssays* **1990**, *12*, 335−340.
(15) Thoma, N. H.; Leadlay, P. F. *Biochem. Soc. Trans.* **1998**, *26*, 293−298.
(16) Waddington, M. D.; Finke, R. G. *J. Am. Chem. Soc.* **1993**, *115*, 4629−4640.
(17) Hay, B. P.; Finke, R. G. *J. Am. Chem. Soc.* **1987**, *109*, 8012−8018.
(18) Chowdhury, S.; Banerjee, R. *Biochemistry* **2000**, *39*, 7998−8006.
(19) Garr, C. D.; Sirovatka, J. M.; Finke, R. G. *J. Am. Chem. Soc.* **1996**, *118*, 11142−11154.
(20) Dong, S. L.; Padmakumar, R.; Banerjee, R.; Spiro, T. G. *J. Am. Chem. Soc.* **1999**, *121*, 7063−7070.
(21) Banerjee, R.; Chowdhury, S. In *Chemistry and Biochemistry of B$_{12}$*; Banerjee, R., Ed.; Wiley-Interscience: New York, 1999.

(22) Mancia, F.; Evans, P. R. *Struct. Fold. Des.* **1998**, *6*, 711−720.
(23) Kräutler, B. *J. Inorg. Biochem.* **2001**, *86*, 65−65.
(24) Scheuring, E.; Padmakumar, R.; Banerjee, R.; Chance, M. R. *J. Am. Chem. Soc.* **1997**, *119*, 12192−12200.
(25) Kozlowski, P. M. *Curr. Opin. Chem. Biol.* **2001**, *5*, 736−743.
(26) Andruniow, T.; Zgierski, M. Z.; Kozlowski, P. M. *Chem. Phys. Lett.* **2000**, *331*, 509−512.
(27) Dolker, N.; Maseras, F.; Lledos, A. *J. Phys. Chem. B* **2003**, *107*, 306−315.
(28) Mancia, F.; Keep, N. H.; Nakagawa, A.; Leadlay, P. F.; McSweeney, S.; Rasmussen, B.; Bosecke, P.; Diat, O.; Evans, P. R. *Structure* **1996**, *4*, 339−350.
(29) Padmakumar, R.; Taoka, S.; Banerjee, R. *J. Am. Chem. Soc.* **1995**, *117*, 7033−7034.
(30) Bouquiere, J. P.; Finney, J. L.; Lehmann, M. S.; Lindley, P. F.; Savage, H. F. J. *Acta Crystallogr., Sect. B* **1993**, *49*, 79−89.
(31) Champloy, F.; Gruber, K.; Jogl, G.; Kratky, C. *J. Synchrotron Radiat.* **2000**, *7*, 267−273.
(32) Champloy, F.; Jogl, G.; Reitzer, R.; Buckel, W.; Bothe, H.; Beatrix, B.; Broeker, G.; Michalowicz, A.; Meyer-Klaucke, W.; Kratky, C. *J. Am. Chem. Soc.* **1999**, *121*, 11780−11789.
(33) Trommel, J. S.; Warncke, K.; Marzilli, L. G. *J. Am. Chem. Soc.* **2001**, *123*, 3358−3366.

actually be due to redox heterogeneity of the cofactor in the enzyme crystal structures, leaving the role of the DMB → His ligand switch with respect to enzymatic Co−C bond activation an open question. Comparison of crystal structures of MMCM in the presence and absence of substrate analogues revealed a major conformational change associated with substrate binding, which led to the proposal that the closure of the active site driven by substrate binding could force displacement of the Ado moiety of the cofactor.[22,34] However, the uncertainties surrounding the oxidation state of the Co ion in the crystal structures make it difficult to ascertain the exact point at which this conformational change occurs, amplifying the need for further spectroscopic study.

To date, MMCM has been the subject of numerous spectroscopic investigations aimed primarily at obtaining qualitative insight into the structure and function of this enzyme. Electronic absorption (Abs) and circular dichroism (CD) spectra of AdoCbl revealed small but notable changes upon cofactor binding to MMCM and upon addition of substrate to holoenzyme.[35] However, as a quantitative interpretation of these changes in terms of geometric and electronic perturbations of the cofactor has thus far been hindered by the lack of a suitable theoretical framework, only limited information could be gleaned from these results. Resonance Raman (RR) vibrational studies by Spiro's group[36] suggested flattening of the corrin ring when AdoCbl binds to MMCM, an interpretation that was consistent with previously published X-ray data (vide supra).[28] These studies also revealed enzyme-induced perturbations of the Co−C bond, as the frequency of ν_{Co-C} was lowered from 430 to 424 cm^{-1} upon AdoCbl binding to apo-MMCM. However, this frequency shift corresponds to a reduction in Co−C BDE by only ∼0.5 kcal/mol.[20] While these results appear to indicate that direct enzyme-induced Co−C bond weakening is insignificant, the extent of Co−C bond activation upon substrate (analogue) binding remains unknown as the associated change in frequency of ν_{Co-C} could not be determined.

With the recent advances in theoretical chemistry and computer technology, it has now become possible to employ high-level density functional theory (DFT) calculations in conjunction with time-dependent DFT (TD-DFT) to analyze Abs and RR data of Cbls using truncated cofactor models that possess the actual corrin ring.[25−27,37−40] A recent publication by our laboratory presented a comprehensive spectroscopic/computational study of the electronic properties of several free Co^{3+}corrinoid species whose axial ligands span a wide range of the spectrochemical series.[40] This study revealed that the TD-DFT method is remarkably successful in reproducing all relevant features in the corresponding Abs spectra. Of particular relevance with respect to present work is that TD-DFT calculations were found to reproduce almost quantitatively the shifts

Chart 1. Structures of the Natural Substrate and Product for MMCM along with Analogues Used in This Study
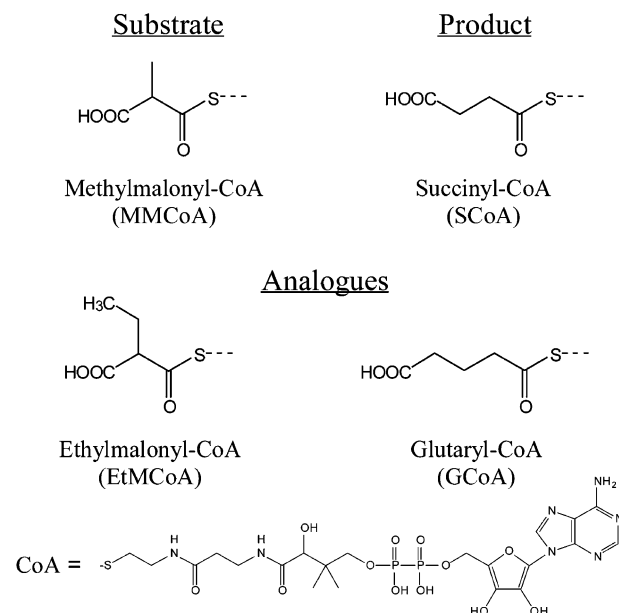
of the α band and the striking intensity redistribution in the γ region in response to axial ligand substitutions. Using this combined spectroscopic/computational methodology as a uniquely sensitive probe of enzyme/cofactor interactions should aid considerably in elucidating the mechanism by which MMCM carries out the exalted trillion-fold rate enhancement for the Co−C bond homolysis reaction.

In this study, Abs and magnetic CD (MCD) spectroscopies were employed to probe the effects of cofactor binding to MMCM and subsequent conversion of the resting (R) state to the substrate-bound (S) and product-bound (P) states (Figure 2) on the electronic structures of the native AdoCbl cofactor and its derivative MeCbl. Due to their different selection rules, these techniques provide complementary information that allows for the resolution and assignment of bands in the optical spectra. Several different substrates shown in Chart 1 were used to generate the S and P states of the enzyme (Figure 2) with both AdoCbl and MeCbl bound to the active site. Observed band shifts upon formation of the R, S, and P states are interpreted within the framework of TD-DFT computational studies that correlate spectral changes with geometric perturbations of the cofactor. Together, these studies provide a direct probe of the structural and electronic properties of the cofactor in its Co^{3+} (i.e., "ground") state as the enzyme progresses through the reaction cycle, allowing for a critical evaluation of enzymatic Co−C bond activation mechanisms proposed in the literature.

2. Experimental Section

Chemicals/Cofactors. AdoCbl, MeCbl, MMCoA, and GCoA were purchased from Sigma and used without further purification. EtMCoA was obtained through the enzymatic reaction of ethylmalonic acid with CoASH catalyzed by malonyl-CoA synthetase[41] and then purified by HPLC using a C$_{18}$ reversed phase column with a gradient from 0% to 30% AcN in 0.1% TFA. The product was confirmed by ^{1}H NMR analysis. The expression vector pKW2 containing the malonyl-CoA synthetase gene with N- and C-terminal His tags was generously provided by Chaitan Khosla (Stanford University) and transformed into

(34) Mancia, F.; Smith, G. A.; Evans, P. R. *Biochemistry* **1999**, *38*, 7999−8005.
(35) Firth, R. A.; Hill, H. A. O.; Pratt, J. M.; Williams, R. J. P.; Jackson, W. R. *Biochemistry* **1967**, *6*, 2178−2189.
(36) Dong, S. L.; Padmakumar, R.; Maiti, N.; Banerjee, R.; Spiro, T. G. *J. Am. Chem. Soc.* **1998**, *120*, 9947−9948.
(37) Andruniow, T.; Kozlowski, P. M.; Zgierski, M. Z. *J. Chem. Phys.* **2001**, *115*, 7522−7533.
(38) Andruniow, T.; Zgierski, M. Z.; Kozlowski, P. M. *J. Phys. Chem. A* **2002**, *106*, 1365−1373.
(39) Andruniow, T.; Zgierski, M. Z.; Kozlowski, P. M. *J. Phys. Chem. B* **2000**, *104*, 10921−10927.
(40) Stich, T. A.; Brooks, A. J.; Buan, N. R.; Brunold, T. C. *J. Am. Chem. Soc.* **2003**, *125*, 5897−5914.

(41) Pohl, N. L.; Hans, M.; Lee, H. Y.; Kim, Y. S.; Cane, D. E.; Khosla, C. *J. Am. Chem. Soc.* **2001**, *123*, 5822−5823.

BL21 DE3 cells. Malonyl-CoA synthetase was purified using Ni-NTA affinity chromatography (Novagen) to higher than 80% homogeneity. The crystalline cofactor samples were dissolved in doubly distilled water at pH 7, while the substrate (analogues) were dissolved in potassium phosphate buffer at pH 7.5 to a concentration of 50 mM.

Purification of Methylmalonyl-CoA Mutase. Recombinant *Propionibacterium shermanii* methylmalonyl-CoA mutase was expressed using the pMEX2/pGP1-2 (provided by Peter Leadlay, Cambridge University) in *Escherichia coli* and was purified as described previously.[42] The specific activity of the enzyme used in this study ranged from 30 to 40 μmol of succinyl-CoA formed/min per mg of protein at 37 °C. Protein concentration was determined by the Bradford method using bovine serum albumin as a standard. Reconstitution of apoenzyme with a 2-fold excess of the native cofactor AdoCbl or the cofactor analogue MeCbl was achieved by incubating MMCM at 4 °C in the dark. Unbound cofactor (analogue) was subsequently removed by gel filtration chromatography on a Micro Bio-Spin P-30 (Bio-Rad) column.

Sample Preparation. All samples used for low-temperature experiments were prepared in 60% (v/v) glycerol glassing agent. Solutions for the free cofactors and MMCM reconstituted with AdoCbl and MeCbl were purged with N_2 gas for 15 min and then injected into MCD sample cells that were immediately frozen in liquid N_2. For the MMCM samples with substrate and substrate analogues, holoenzyme was purged with N_2 and then mixed with at least a 40-fold molar excess of the appropriate substrate (analogue). With K_d values for the substrate (analogues) ranging from 49 μM (EtMCoA[20]) to 121 μM (MMCoA[18]), this substrate/protein ratio and the high protein concentrations used (ranging from 0.1 to 0.5 mM, as determined spectrophotometrically at 300 K on the basis of published molar extinction coefficients) ensured complete conversion to the substrate-bound form of holoenzyme. Samples were frozen in liquid N_2 within 2 min of substrate (analogue) addition to quench reactions that are slow on this time scale. All enzyme samples were handled under reduced light to prevent undesired photolysis of the cofactor's Co–C bond.

Spectroscopy. Electronic Abs, CD, and MCD spectra were obtained using a Jasco J-715 spectropolarimeter in conjunction with an Oxford Instruments SM-4000 8T magnetocryostat. All MCD spectra reported in this paper were obtained by subtracting the −7 T spectrum from the +7 T spectrum to eliminate contributions from the natural CD. Consistent with the diamagnetic nature of all cofactors states investigated herein, MCD spectra obtained on any given sample at 4.5, 10, 25, and 50 K were superimposable. Room-temperature Abs spectra for all samples were obtained using a Varian Cary 5e spectrophotometer.

Computational Models. An approximate model for MeCbl was generated starting from the corresponding highest-resolution X-ray data reported to date,[43] with the DMB base modeled as an imidazole (preserving the original Co–N_{ax} bond length) and the entire nucleotide loop replaced by a hydrogen atom at C^{17}. All other corrin ring substituents were substituted by H atoms separated by 1.1 Å from the neighboring C atoms. This MeCbl model was previously shown to reproduce all the essential electronic features of the actual cofactor.[40] For the systematic variation of the axial bond lengths, all atoms were kept frozen except those of the axial ligand whose positions were to be optimized as a function of the bond distance between the Co and the other (i.e., trans) axial ligand. To generate MeCbl models that differed with respect to their fold angles, two carbon atoms residing on opposite sides of the macrocycle were fixed at the desired distance and all other atoms were geometry optimized (see section 3.3, Computational Data for details). Because in this case the macrocycle was optimized in the absence of the full DMB ligand, flattening of the corrin ring relative to the experimental structure was observed due to the relaxation of steric constraints imposed by the bulkier DMB in the actual cofactor.[44]

The geometries were optimized by DFT energy minimization using the Amsterdam Density Functional (ADF) 2000.01 suite of programs.[45,46] All optimizations were carried out on a home-built cluster consisting of 20 Intel Xeon processors using ADF basis set IV, an integration constant of 4.0, and the Vosko-Wilk-Nusair local density approximation (VWN-LDA)[47] with the nonlocal gradient corrections of Becke for exchange[48] and Perdew for correlation.[49] Core orbitals were frozen through 1s (C, N, O) and 3p (Co). The SCF convergence criterion used was 1×10^{-6} hartrees. Geometries were considered converged when the change in energy between subsequent cycles dropped below 1×10^{-3} hartrees and when the maximum gradient was less than 0.005 hartree/Å for the trans axial ligand optimizations and 0.01 hartree/Å for the fold angle variations. Atomic coordinates for all DFT geometry-optimized models presented in the text can be found in the Supporting Information (Tables S1–S30).

Single-Point DFT Calculations. Single-point DFT calculations were performed using the ORCA 2.2 software package developed by Dr. Frank Neese (MPI Mülheim, Germany).[50] Becke's three-parameter hybrid functional for exchange[51,52] combined with the Lee–Yang–Parr correlation functional[53] (B3LYP/G) using the default 20% Hartree–Fock exchange were employed. The SV(P) (Ahlrichs polarized split valence) basis[54,55] in conjunction with the SV/C auxiliary basis[56] were used for all atoms except Co, for which the more accurate TZVP basis was utilized.[56,57] The default SCF convergence criterion of 1×10^{-6} hartrees was used for all calculations. The size of the integration grid used in all calculations was 3 (Lebedev 194 points).

TD-DFT Calculations. Transition dipole moments and vertical excitation energies for all models were calculated by the TD-DFT method[58–60] within the Tamm–Dancoff approximation[61,62] as implemented in ORCA 2.2, employing the hybrid functional and basis sets described above. To achieve convergence of the TD-DFT calculations, the resolution of the identity approximation was used to evaluate the Coulomb term.[63] For each model, 40 excited states were calculated by including all one-electron excitations within an energy window of ±3 hartrees with respect to the HOMO/LUMO energies. To compensate for the fact that the B3LYP TD-DFT method tends to overestimate transition energies,[37,60] all simulated spectra were red-shifted by 4000 cm^{-1}. From the 40 excited states, electron density difference maps (EDDMs) were created for the states that produce the greatest contributions to the calculated Abs spectrum. The gOpenMol program developed by Laaksonen[64] was used to generate isosurface plots for

(44) Experimental fold angle, $\theta = 14.76°$; optimized His model, $\theta = 5.73°$; optimized DMB model, $\theta = 9.25°$. While the model containing the full DMB agrees better with the experimental structure, it was too large to be treated with TD-DFT at the level of theory necessary to produce accurate simulated spectra.
(45) Baerends, E. J.; Ellis, D. E.; Ros, P. *Chem. Phys.* **1973**, *2*, 41–51.
(46) te Velde, G.; Baerends, E. J. *J. Comput. Phys.* **1992**, *99*, 84–98.
(47) Vosko, S. H.; Wilk, L.; Nusair, M. *Can. J. Phys.* **1980**, *58*, 1200–1211.
(48) Becke, A. D. *J. Chem. Phys.* **1986**, *84*, 4524–4529.
(49) Perdew, J. P. *Phys. Rev. B* **1986**, *33*, 8822–8824.
(50) Neese, F. *ORCA*, version 2.2; an ab initio, density functional, and semiempirical program package; Max-Planck-Institut für Bioanorganische Chemie: Mülheim an der Ruhr, Germany, 2001.
(51) Becke, A. D. *J. Chem. Phys.* **1993**, *98*, 1372–1377.
(52) Becke, A. D. *J. Chem. Phys.* **1993**, *98*, 5648–5652.
(53) Lee, C.; Yang, W.; Parr, R. G. *Phys. Rev. B* **1988**, *37*, 785–789.
(54) Ahlrichs, R., unpublished results.
(55) Schäfer, A.; Horn, H.; Ahlrichs, R. *J. Chem. Phys.* **1992**, *97*, 2571–2577.
(56) The Ahlrichs auxiliary basis sets were obtained from the TurboMole basis set library under ftp.chemie.uni-karlsruhe.de/pub/cbasen. Weigend, F.; Haeser, M. *Theor. Chem. Acc.* **1997**, *97*, 331–340.
(57) Schäfer, A.; Huber, C.; Ahlrichs, R. *J. Chem. Phys.* **1994**, *100*, 5829–5835.
(58) Bauernschmitt, R.; Ahlrichs, R. *Chem. Phys. Lett.* **1996**, *256*, 454–464.
(59) Casida, E. M.; Jamorski, C.; Casida, K. C.; Salahub, D. R. *J. Chem. Phys.* **1998**, *108*, 4439–4449.
(60) Stratman, R. E.; Scuseria, G. E.; Frisch, M. J. *J. Chem. Phys.* **1998**, *109*, 8218–8224.
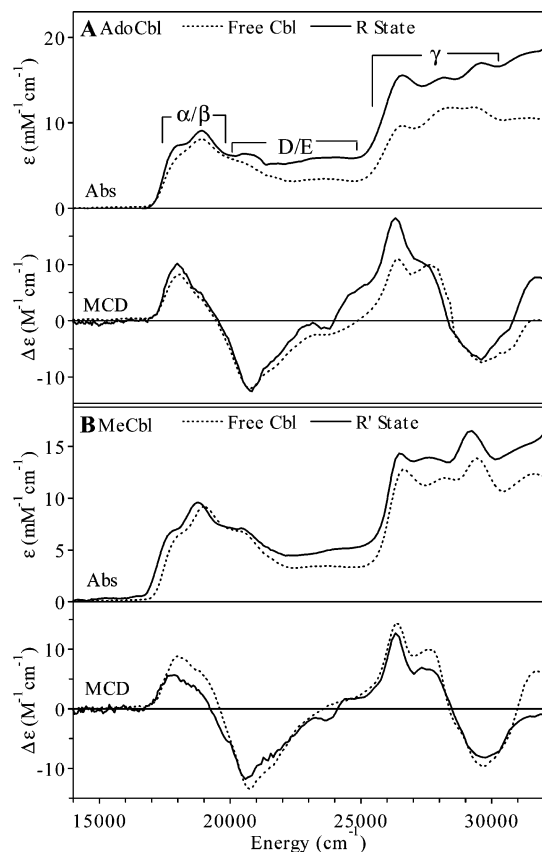(61) Hirata, S.; Head-Gordon, M. *Chem. Phys. Lett.* **1999**, *302*, 375–382.
(62) Hirata, S.; Head-Gordon, M. *Chem. Phys. Lett.* **1999**, *314*, 291–299.
(63) Neese, F.; Olbrich, G. *Chem. Phys. Lett.* **2002**, *362*, 170–178.
(64) Laaksonen, L. *J. Mol. Graphics* **1992**, *10*, 33–34.

(42) Padmakumar, R.; Banerjee, R. *J. Biol. Chem.* **1995**, *270*, 9295–9300.
(43) Rossi, M.; Glusker, J. P.; Randaccio, L.; Summers, M. F.; Toscano, P. J.; Marzilli, L. G. *J. Am. Chem. Soc.* **1985**, *107*, 1729–1738.

Figure 3. 4.5 K Abs and 25 K MCD spectra of free and MMCM-bound AdoCbl (A) and MeCbl (B). Band designations are given for AdoCbl.

the calculated molecular orbitals (MOs) and EDDMs with isodensity values of 0.03 b^{-3} and 0.003 b^{-3}, respectively.

3. Results and Analysis

3.1. Spectroscopic Data. (i) Resting State. Figure 3 shows electronic absorption (Abs), circular dichroism (CD), and magnetic CD (MCD) spectra for free and MMCM-bound AdoCbl (top) and MeCbl (bottom). Consistent with the diamagnetic nature of all cofactor species studied herein, MCD spectra of any given sample were found to be temperature independent; thus, only the 25 K spectra are shown. In a recent publication, our laboratory presented a detailed spectroscopic and computational study on free Co^{3+}corrinoid species cofactors in which AdoCbl and MeCbl were shown to exhibit nearly identical electronic spectra despite the steric differences in their upper axial ligands. This close resemblance is due in large part to the comparable electron-donating properties of the upper axial ligands (5′-deoxyadenosine and methyl, respectively), with both ligands known to be strong σ-donors. Thus, comparison of spectroscopic data of MMCM reconstituted with AdoCbl and the non-native MeCbl cofactor provides a convenient way to evaluate contributions from the Ado moiety to cofactor/active site interactions and their effect on the Co−C bond properties at various stages along the reaction pathway. Additionally, the sterically less constrained MeCbl cofactor allows for the possibility of observing corrin ring deformations in the enzyme active site that may not be detected using AdoCbl where the bulky Ado moiety potentially impedes the upward folding of the macrocycle.

(a) AdoCbl. The spectroscopic results for the free and MMCM-bound (R state, Figure 2) native cofactor are shown in Figure 3A. Our Abs spectra agree well with those reported in the literature,[65] indicating that neither addition of glycerol nor sample freezing perturb the cofactor to any significant degree. Definitive assignments for all major bands observed in the Abs spectra of free alkyl-Co^{3+}Cbls were presented recently by our laboratory[40] and are briefly summarized herein to establish a reference point for the analysis of spectral data obtained for the enzyme-bound cofactors. The Abs spectrum of AdoCbl (and alkyl-Co^{3+}Cbls in general) is characterized by a broad, prominent feature at low energy, the so-called α,β region, and several bands of greater intensity at higher energy, designated as the γ region (Figure 3A, top). The α and β bands were identified as the origin and first member of a vibronic progression associated with the corrin-based HOMO → LUMO (i.e., π → π*) transition that is polarized primarily along the long axis of the corrin macrocycle (defined by the C^5···C^{15} vector, Figure 1). The fact that a derivative-shaped feature appears in the α/β region of the MCD spectrum of AdoCbl indicates that the prominent shoulder on the high-energy side of the β band in the AdoCbl Abs spectrum corresponds to the origin of a distinct corrin π → π* electronic transition that is partially short-axis polarized (Co···C^{10} vector, Figure 1). The γ region of the AdoCbl Abs spectrum contains several overlapping bands of similar intensity that have been ascribed to multiple corrin-centered transitions having varying degrees of short-axis and long-axis polarization.

Although the Abs spectra of Co^{3+}Cbls are dominated by corrin π → π*-based transitions, they are considerably affected by the upper axial ligand. In the case of alkyl-Co^{3+}Cbls, the strong σ-donating character of the alkyl group gives rise to a dramatic destabilization of the filled Co 3d orbitals, raising them sufficiently high in energy to allow for significant mixing with the frontier orbitals of the corrin macrocycle. This increased contribution from the Co 3d orbitals to the corrin π-based MOs provides a means of communication between the axial ligands and the corrin macrocycle that would potentially allow for activation of the axial Co−C bond through corrin ring distortions. DFT geometry optimizations coupled to TD-DFT spectral calculations that evaluate this intriguing possibility are presented in section 3.3, Computational Data.
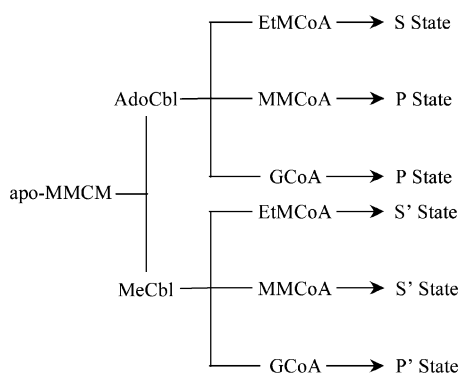
Qualitative comparison of the two sets of spectra presented in Figure 3A discloses few modifications upon binding of the AdoCbl cofactor to apo-MMCM. The only notable changes are (i) an increase in the Abs intensity that has previously been attributed to the decreased dielectric constant in the enzyme active site relative to H$_2$O,[65] and (ii) band sharpening across the entire UV/visible spectral range in both the Abs and theMCD spectra. This band sharpening suggests that the cofactor adopts a well-defined conformation in the MMCM active site, possibly through stabilization of one of the several roughly isoenergetic orientations of the Ado moiety that exist in solution.[66,67] In light of the fact that the intramolecular DMB that coordinates to Co in the lower axial position of the free cofactor is displaced by a histidine residue from the enzyme active site upon AdoCbl binding to the apoenzyme, it is quite remarkable that the associated spectral changes are so minor. This result suggests

(65) Chowdhury, S.; Banerjee, R. *Biochemistry* **1999**, *38*, 15287−15294.
(66) Marques, H. M.; Zou, X.; Brown, K. L. *J. Mol. Struct.* **2000**, *520*, 75−95.
(67) Marques, H. M.; Brown, K. L. *Coord. Chem. Rev.* **2002**, *225*, 123−158.

Chart 2. Flow Chart Illustrating the Final States Obtained upon Addition of the Substrate (Analogues) to apo-MMCM Reconstituted with Either AdoCbl (Upper) or MeCbl (Lower)

Figure 4. Comparison of 4.5 K Abs and 25 K MCD spectra for the R, S, and P states of AdoCbl (A) and the R′, S′, and P′ states of MeCbl (B).

that the DMB → His axial ligand switch has insignificant effects on the cofactor's electronic structure, although changes in Co—C bonding cannot necessarily be ruled out on the basis of these data alone as the AdoCbl Abs spectrum is dominated by corrin $\pi \rightarrow \pi^*$-based transitions.

(b) MeCbl. The low-temperature Abs and MCD spectra of free and MMCM-bound (R′ state, Figure 2) MeCbl are shown in Figure 3B. The two sets of spectra are strikingly similar and bear close resemblance to those of free and enzyme-bound AdoCbl (Figure 3A), indicating that the geometric and electronic properties of MeCbl also change little upon cofactor binding to MMCM.[68] Interestingly, however, comparison of the data in Figure 3 reveals that the spectral differences between the free and enzyme-bound states are considerably larger for MeCbl than for AdoCbl, which is particularly evident for the α,β bands and the high-energy features in the γ region. A quantitative evaluation of these band shifts is presented in section 3.2, Spectral Analysis, and their electronic origin and structural implications are explored in section 3.3, Computational Data.

(ii) Substrate and Product States. The substrate-bound (S) and product-bound (P) states of holo-MMCM were investigated using the actual substrate as well as the substrate and product analogues shown in Chart 1. In each case, the substrate (analogue) was added to the holoenzyme and the resulting mixture was frozen in liquid N_2 within 2 min. Addition of MMCoA to MMCM reconstituted with AdoCbl and MeCbl leads to the formation of the P state and the S′ state, respectively, as turnover is extremely rapid with the former species[69] but nonexistent with the latter. Although EtMCoA is competent to induce Co—C bond cleavage of MMCM-bound AdoCbl, the rearrangement reaction is slowed by 3−4 orders of magnitude relative to the MMCoA → SCoA conversion.[70,71] This increased reaction time results in negligible rearrangement on the time scale of sample preparation, thus allowing for spectroscopic investigation of the S (or S′) state when holoenzyme is incubated with EtMCoA. Finally, GCoA is a slow product analogue that undergoes turnover on the order of days;[72] thus, incubation of
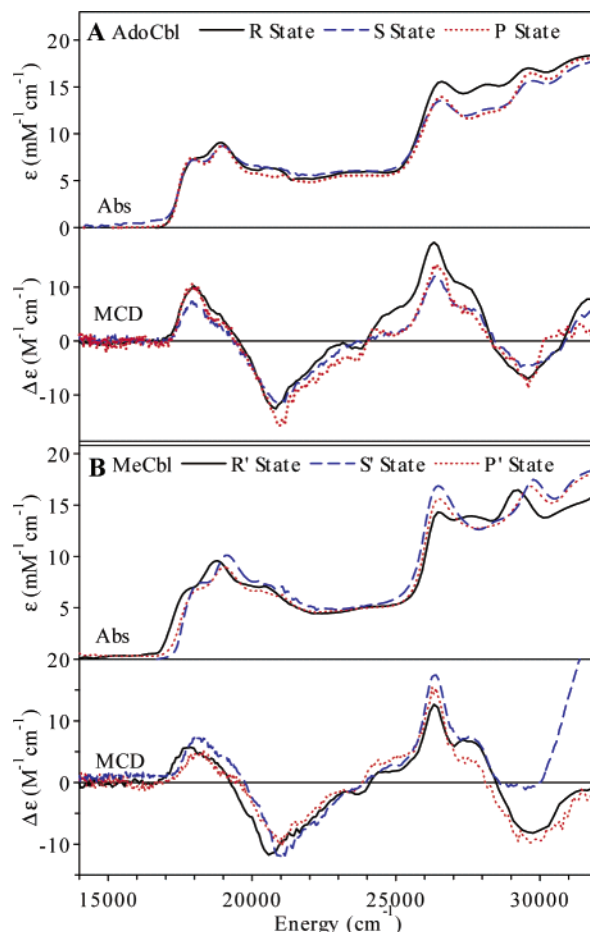
holoenzyme with GCoA leads to the formation of the P (or P′) state. These reactions are summarized in Chart 2.

(a) AdoCbl. The Abs and MCD spectra for the S and P states obtained using EtMCoA and MMCoA, respectively, are compared with the R state spectra in Figure 4A (P state spectra obtained with GCoA are nearly identical to those shown in Figure 4A, see Figure S1, Supporting Information). The three sets of spectra are remarkably similar to each other and to the spectra of free AdoCbl (Figure 3A). The only noticeable change upon conversion of the R state to the S and P states corresponds to a modest increase in spectral resolution that also accounts for the small increase in intensity of the MCD features at low energy (α/β and D/E regions). The identical nature of the S and P state spectra is consistent with X-ray crystal structures that show essentially identical atomic positions for the protein when substrate or product is bound.[73] These results are also in line with previous RR studies that revealed negligible changes in the corrin ring modes and only a small intensity transfer from the Co—C stretching mode to the Co—C—C bending mode upon R → S state conversion.[20] Overall, these data indicate that the electronic structure of the native AdoCbl cofactor is not significantly perturbed even in the presence of substrate and product (analogues).

(b) MeCbl. Parallel studies were performed to investigate the S′ and P′ states with the cofactor analogue MeCbl bound to

(68) Note that the spectra of free and enzyme-bound MeCbl are similarly well-resolved and comparable in resolution to those of MMCM-bound AdoCbl, lending credence to our hypothesis that the band sharpening observed in the AdoCbl spectra upon enzyme binding reflects the selection of a single orientation of the Ado moiety in the active site.
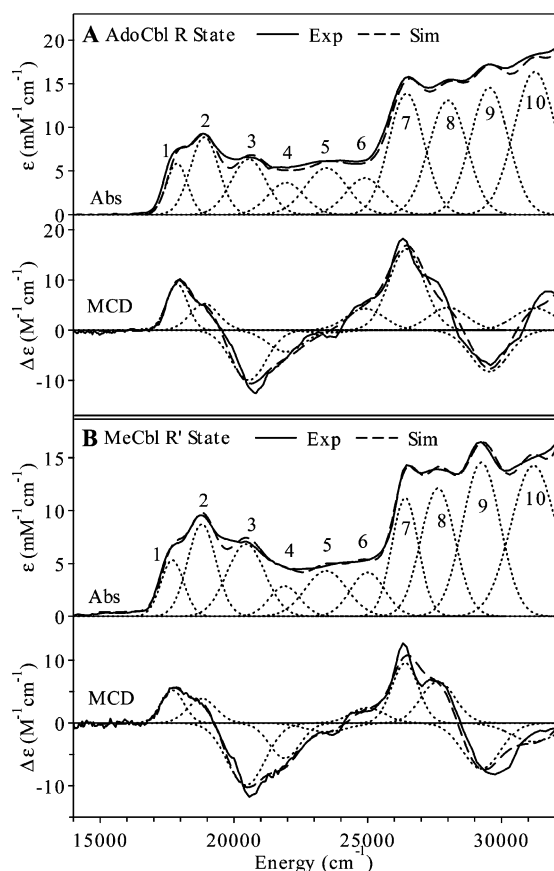(69) Meier, T. W.; Thoma, N. H.; Leadlay, P. F. *Biochemistry* **1996**, *35*, 11791−11796.
(70) Retey, J. S., E. H.; Zagalak, B. *Eur. J. Biochem.* **1978**, *83*, 437−451.
(71) Abend, A.; Illich, V.; Retey, J. *Eur. J. Biochem.* **1997**, *249*, 180−186.
(72) Padmakumar, R.; Banerjee, R. *Biofactors* **1995**, *5*, 83−86.

(73) Evans, P. R.; Mancia, F. In *Vitamin B₁₂ and B₁₂ Proteins*; Krautler, B., Augoni, D., Golding, B. T., Eds.; Wiley-Interscience: New York, 1998; pp 217−226.

Figure 5. Solid lines: 4.5 K Abs and 25 K 7 T MCD spectra of the AdoCbl R state (A) and the MeCbl R′ state (B). Dotted lines: Gaussian deconvolutions of the experimental spectra obtained with the fit parameters in Table 1. Broken lines: Sum of individual Gaussian bands.

Table 1. Fit Parameters from Gaussian Deconvolutions of the Abs and MCD Spectra of the Free Cofactor, holo-MMCM, and MMCoA Treated with holo-MMCM for AdoCbl (Top) and MeCbl (Bottom)[a] (Bands Shifts of Greater than 100 cm⁻¹ Are Assumed To Be outside the Realm of Experimental Error and Are Highlighted in Bold)

	peak positions (cm⁻¹)			band shifts (cm⁻¹)	
peak	AdoCbl	R state	P state (SCoA)	Δ enzyme binding	Δ SCoA binding
1	17 875	17 875	17 875	0	0
2	18 850	18 900	19 000	50	100
3	**20 500**	**20 550**	**20 700**	**50**	**150**
4	**21 950**	**21 950**	**22 100**	**0**	**150**
5	23 500	23 450	23 400	−50	−50
6	25 000	24 900	24 900	−100	0
7	26 450	26 450	26 425	0	−25
8	27 950	28 000	27 950	50	−50
9	**29 400**	**29 550**	**29 650**	**150**	**100**
10	31 300	31 250	31 250	−50	0

			S′ state (MMCoA)	Δ enzyme binding	Δ MMCoA binding
peak	MeCbl	R′ state			
1	**17 870**	**17 700**	**18 150**	**−170**	**450**
2	**18 950**	**18 800**	**19 200**	**−150**	**400**
3	**20 500**	**20 450**	**20 700**	**−50**	**250**
4	21 800	21 900	21 950	100	50
5	23 450	23 450	23 400	0	−50
6	24 950	24 900	24 850	−50	−50
7	**26 600**	**26 400**	**26 500**	**−200**	**100**
8	**28 050**	**27 625**	**28 300**	**−425**	**675**
9	**29 550**	**29 250**	**29 850**	**−300**	**600**
10	**31 600**	**31 200**	**31 400**	**−400**	**200**

[a] Note that addition of MMCoA to MMCM reconstituted with AdoCbl and MeCbl leads to the formation of the P state and the S′ state, respectively, as turnover is extremely rapid with the former species[69] but nonexistent with the latter.

MMCM. Low-temperature Abs and MCD spectra for these states, along with R′ state data, are shown in Figure 4B (S′ state spectra obtained with MMCoA are very similar to those in Figure 4B, see Figure S1). The S′ and P′ states, similar to the S and P states, also exhibit nearly identical Abs and MCD spectra, with the α,β-region of the P′ state slightly red-shifted as compared to that of the S′ state. Most importantly, however, the bands that were observed to red-shift upon binding of MeCbl to apoenzyme (Figure 3B) display significant blue-shifts upon conversion of the R′ state to the S′ and P′ states. Therefore, as compared to the native cofactor AdoCbl, changes in the electronic structure of the sterically less constrained MeCbl cofactor upon binding to MMCM and treatment of holoenzyme with substrate and product (analogues) are much more substantial.

3.2. Spectral Analysis. To quantify the band shifts observed in the Abs and MCD spectra presented above, each data set was fit with the fewest possible number of Gaussian bands required to adequately reproduce the major features in the experimental spectra. The MCD spectra were fit first as they are better resolved than the corresponding Abs spectra. Subsequently, the band positions and widths were adjusted iteratively to achieve the best simultaneous fit of the Abs and MCD spectra. Representative examples of these fits are shown in Figure 5 (see Figures S2 and S3 for the other species included in this study).

(a) AdoCbl. The Gaussian-resolved Abs and MCD spectra for the R state are shown in Figure 5A, and the relevant results

from spectral deconvolutions for this state, the free cofactor, and the P state are summarized in Table 1 (S state data are identical within experimental error to those reported for the P state and are thus not shown). Ten Gaussian bands were required to accurately reproduce the major spectral features in all three sets of spectra. As the overall shapes of the Abs and MCD spectra do not vary greatly from species to species, a direct comparison between the Gaussian band positions can be made to quantify the observed band shifts associated with cofactor binding to MMCM and substrate (analogue) binding to holo-enzyme. Band shifts up to $|\Delta| \approx 100$ cm⁻¹ are considered within experimental error and therefore do not necessarily indicate a change in the electronic structure of the cofactor. From Table 1, only three bands in the AdoCbl spectra exhibit shifts outside the experimental uncertainties. Band 9 blue-shifts by ~150 cm⁻¹ upon R state formation and another 100 cm⁻¹ upon addition of MMCoA to produce the P (and S) state. Bands 3 and 4 also shift to higher energy, both moving ~150 cm⁻¹ from their R state position upon MMCoA binding. These changes, while outside the realm of experimental error, reveal that the electronic properties of the free AdoCbl cofactor are virtually unperturbed in the R, S, and P states.

(b) MeCbl. The MeCbl Abs and MCD spectra also required 10 Gaussian bands to achieve a satisfactory fit (Figure 5B). The band positions obtained from spectral deconvolutions for the free, R′, and S′ MeCbl states (Table 1; P′ state data are not shown as they are very similar to those reported for the S′ state) reveal that, in comparison to the AdoCbl data, the MeCbl spectra show significantly greater band shifts with a maximum Δ value of 675 cm⁻¹. All bands in both the α,β region and the γ region

exhibit red-shifts upon enzyme binding, with bands 1 and 2 shifting by ~ -150 cm^{-1} and bands 7−10 shifting between −200 and −425 cm^{-1}. These shifts to lower energy are in direct contrast to the blue-shifting of the same bands observed upon AdoCbl binding to MMCM. Addition of MMCoA to holo-enzyme reconstituted with MeCbl to produce the S′ state is accompanied by blue-shifts of bands 1−3 and 7−10, with the most significant changes occurring for bands 1, 2, 8, and 9. With Δ values for these bands between 400 and 600 cm^{-1}, it is evident that the electronic structure of the sterically less constrained MeCbl cofactor is considerably more perturbed by the enzyme environment, particularly in the presence of substrate or product. A quantitative analysis of these band shifts within the framework of electronic structure calculations is presented next.

3.3. Computational Data. In this section, results from DFT and TD-DFT calculations are presented that build upon our spectroscopically validated bonding descriptions for the free Co^{3+}Cbl cofactors developed recently.[40] By using TD-DFT, spectral changes associated with geometric perturbations of the Co^{3+}Cbl structure can be evaluated to establish a spectro/structural correlation. On the basis of this correlation, experimentally observed band shifts accompanying the formation of the various enzymatic states discussed above can then be interpreted within the context of cofactor/active site interactions.

The spectroscopic data presented above suggest that the MeCbl cofactor is a more sensitive probe of alterations in the enzyme active site, perhaps due to the increased flexibility of the corrin macrocycle in the absence of the bulky Ado moiety. This increased sensitivity along with the computationally more accessible size led us to focus on MeCbl rather than AdoCbl for the computational studies presented herein (their implications with respect to the AdoCbl/MMCM system will be explored in the Discussion). The cofactor model used was based on the crystal structure geometry for MeCbl, utilizing the same truncation scheme that previously afforded excellent agreement between calculated and experimental spectroscopic results (see section 2, Experimental Section).

(i) MeCbl Electron Density Difference Maps. To obtain novel insight into the nature of the electronic transitions that dominate the MeCbl Abs spectrum (and alkyl-Co^{3+}Cbl spectra in general), electron density difference maps (EDDMs) were generated on the basis of the TD-DFT results for the MeCbl model.[74] These EDDMs provide a visual representation of the change in electron density across the cofactor associated with each transition. On the basis of the results summarized in Table 1, analysis of the transitions responsible for bands 1−3 and 7−10 is of particular interest, as these bands are most strongly affected by the protein. From Figure 6 (bottom), the α/β EDDM associated with the single electronic transition giving rise to bands 1 and 2 (the vibronic progression known as the α/β bands) reveals a significant loss of electron density in the Co−C bonding region and a pattern of alternating electron density gain and loss across the conjugated portion of the macrocycle, indicative of a corrin based $\pi \rightarrow \pi^*$ transition that nonetheless significantly weakens the Co−C bond. Thus, this EDDM provides an intuitively appealing explanation as to why RR
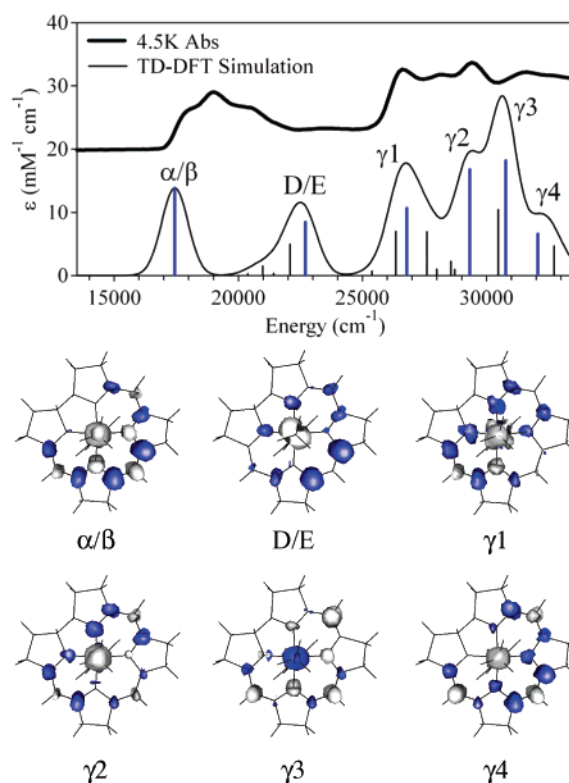
Figure 6. Top: Comparison of the experimental and TD-DFT simulated Abs spectra for MeCbl. Bottom: Electron density difference maps (EDDMs) for the transitions producing the greatest contributions to the Abs spectrum.

spectra obtained upon excitation in resonance with the α/β bands exhibit significant enhancement of ν_{Co-C} in addition to corrin-based normal modes.[20,40,75] The γ2 and γ4 EDDMs (correlating with bands 8 and 10 in the experimental Abs spectrum, Figure 5B) exhibit the same characteristics as the α/β EDDM, which concurs nicely with the observation that, in the experimental spectra, all these bands exhibit moderate red-shifts upon MeCbl binding to MMCM and rather large blue-shifts upon substrate (analogue) binding to the holoenzyme (Table 1). The transitions that contribute to band 3 (D/E EDDM) and band 7 (γ1 EDDM) are best characterized as metal-to-ligand charge-transfer (MLCT) excitations with a significant loss of electron density around the metal center and a fairly uniform gain of electron density across the conjugated π system of the macrocycle.[76] These bands are largely unaffected by MeCbl binding to MMCM and show some of the smallest shifts upon substrate binding to holo-enzyme. Consequently, the MOs involved in these transitions are expected to be largely unperturbed in the enzymatic ground state. Finally, the transition responsible for band 9 (γ3 EDDM) has predominant ligand-to-metal charge-transfer (LMCT) character; it is the only transition of this type to contribute markedly to the MeCbl Abs spectrum.

(ii) Spectro/Structural Correlations. Clearly, the absence of major differences in the electronic spectra of free and enzyme-bound AdoCbl alone is insufficient to definitively rule out protein-induced perturbations of the cofactor's Co−C bond in the Co^{3+} (i.e., "ground") state, as the dominant transitions are

(74) It was not possible to generate EDDMs in the previous version of *ORCA* that was used in our earlier computational studies of the free Co^{3+}corrinoids (see ref 40).

(75) Dong, S. L.; Padmakumar, R.; Banerjee, R.; Spiro, T. G. *Inorg. Chim. Acta* **1998**, *270*, 392−398.

(76) Note that the formal Co^{4+} oxidation state in these MLCT excited states is stabilized by substantial charge donation from the alkyl group to the cobalt center.

Table 2. Results from Partial DFT Geometry Optimizations for the MeCbl Model in Which One Axial Bond Length Was Fixed at the Desired Value and the Energy Was Minimized with Respect to the Trans Axial Ligand[a]

fixed r(Co–C) (Å)	opt r(Co–N$_{ax}$) (Å)	relative E (kcal/mol)
1.60	2.281	39.96
1.70	2.247	18.72
1.80	2.233	6.82
1.90	2.215	1.27
1.98	2.203	0.00
2.02	2.196	0.11
2.10	2.182	1.37
2.20	2.167	4.38
2.30	2.166	8.55
2.40	2.156	13.00

fixed r(Co–N$_{ax}$) (Å)	opt r(Co–C) (Å)	relative E (kcal/mol)
1.81	2.026	14.50
1.91	2.016	6.64
2.01	2.005	2.44
2.11	2.000	0.54
2.16	1.998	0.12
2.21	1.996	0.00
2.31	1.994	0.25
2.41	1.992	0.99
2.51	1.990	1.92
2.61	1.990	3.02

[a] Experimental structure values: MeCbl,[77] r(Co–C) = 1.979 Å, r(Co–N$_{ax}$) = 2.163 Å; AdoCbl,[30] r(Co–C) = 2.030 Å, r(Co–N$_{ax}$) = 2.203 Å.

primarily corrin $\pi \rightarrow \pi^*$ in character. Thus, although unlikely, it is feasible for such perturbations to occur without significantly altering band shapes and positions. The observation of changes in the electronic structure of the cofactor analogue MeCbl under identical conditions suggests that sizable interactions between the enzyme and the cofactor do in fact occur and may serve to activate the Co–C bond to a small degree, but in a manner that is not apparent with the structurally more constrained AdoCbl cofactor. To explore the nature of these interactions, a combined spectroscopic/computational methodology was developed that correlates spectral changes with structural perturbations of the cofactor. Generation of this correlation was achieved through TD-DFT calculations on MeCbl models in which the axial Co–C and Co–N$_{ax}$ bond lengths as well as the corrin fold angle were systematically varied, as described below.

(a) Axial Bond Lengths. A series of TD-DFT calculations were performed in which the Co–C and Co–N$_{ax}$ bond lengths of the MeCbl model were systematically varied up to ±0.4 Å from their equilibrium distances of r(Co–C) = 1.98 Å and r(Co–N$_{ax}$) = 2.16 Å.[77] In each case, one axial bond length was fixed at the desired value, and a partial geometry optimization was then performed to minimize the energy with respect to the atomic coordinates of the trans axial ligand while all atoms in the corrin macrocycle were kept frozen. The relevant results from these calculations are summarized in Table 2 along with representative crystallographic data for AdoCbl and MeCbl.

These partial geometry optimizations provide useful insight into the nature of the axial bonding interactions of the cofactor. As the Co–C bond distance increases from 1.60 to 2.40 Å, the optimized Co–N$_{ax}$ bond length decreases considerably from 2.281 to 2.156 Å, producing a correlation characteristic of a normal trans effect. This result is understood in terms of the fact that the degree of Co–N$_{ax}$ σ-antibonding character is
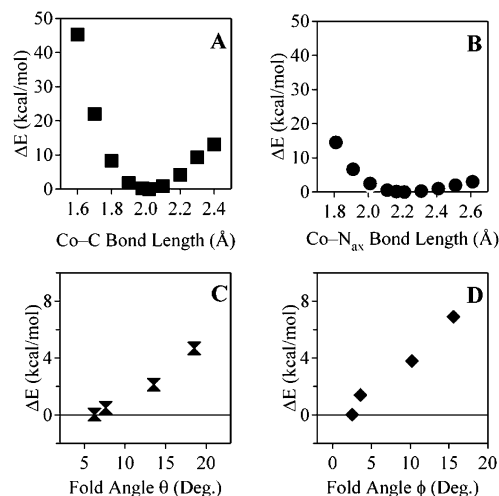
Figure 7. Calculated potential energy surfaces (PESs) for the MeCbl cofactor with the following structural perturbations: (A) Co–C bond length, (B) Co–N$_{ax}$ bond length, (C) fold angle θ, (D) fold angle ϕ.

directly determined by the extent of σ-donation of electron density from the upper axial ligand into the (empty) Co 3d$_{z^2}$ orbital. As the Co–C bond increases, this induced Co–N$_{ax}$ σ-antibonding interaction decreases, allowing the lower axial ligand to approach the Co center. Alternatively, altering the Co–N$_{ax}$ bond distance by a total of 0.8 Å gives rise to a total spread in the optimized Co–C bond lengths of merely 0.036 Å. Thus, while modulation of the Co–C bond distance considerably affects the bonding interaction between the Co center and the lower axial nitrogen donor ligand, changes in the lower axial ligand position have virtually no effect on the Co–C bond strength. This somewhat counterintuitive behavior, which however is anticipated on the basis of the axial ligand bonding scheme developed in our studies of free Co^{3+}corrinoids,[40] is consistent with experimental RR data that also indicate little to no change in the Co–C bond strength upon changing the lower axial ligand.[75]

Potential energy surfaces (PESs) associated with these two axial distortions (Figure 7, panels A and B) indicate that even small changes in the Co–C bond distance are energetically very demanding, arguing against the involvement of a direct protein-induced weakening of the Co–C bond to any significant degree. Alternatively, variations in the axial Co–N$_{ax}$ bond distance over a large range require relatively little energy (note that this result is consistent with a recent computational study performed by Kozlowski and co-workers,[78] which appeared while this paper was in review), suggesting that stabilization of an unusually long Co–N$_{ax}$ bond in the protein active site would be feasible on the basis of energetic considerations. However, as changes in the lower axial ligand position have virtually no effect on the Co–C bond strength (Table 2), proposals of Co–C bond activation mechanisms invoking the lower axial ligand are not supported by our data.

Figures 8 and 9 show representative TD-DFT calculated Abs spectra for the various MeCbl models that differ with respect to their Co–C and Co–N$_{ax}$ bond lengths (i.e., a subset of the models included in Table 2). The lowest-energy band (the α/β transition, Figure 6) is predicted to move significantly as a

(77) Randaccio, L.; Furlan, M.; Geremia, S.; Slouf, M.; Srnova, I.; Toffoli, D. *Inorg. Chem.* **2000**, *39*, 3403–3413.

(78) Freindorf, M.; Kozlowski, P. M. *J. Am. Chem. Soc.* **2004**, *126*, 1928–1929.
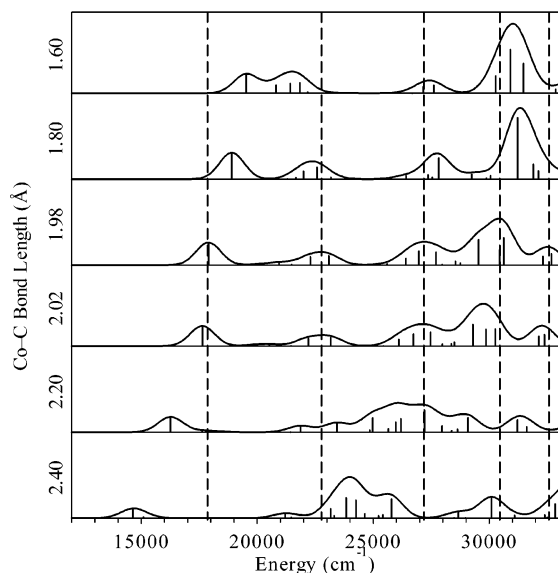
Figure 8. Selected TD-DFT simulated Abs spectra for MeCbl models with fixed upper axial bond lengths between 1.60 and 2.40 Å. Relevant structural parameters for these optimized models are given in Table 2.
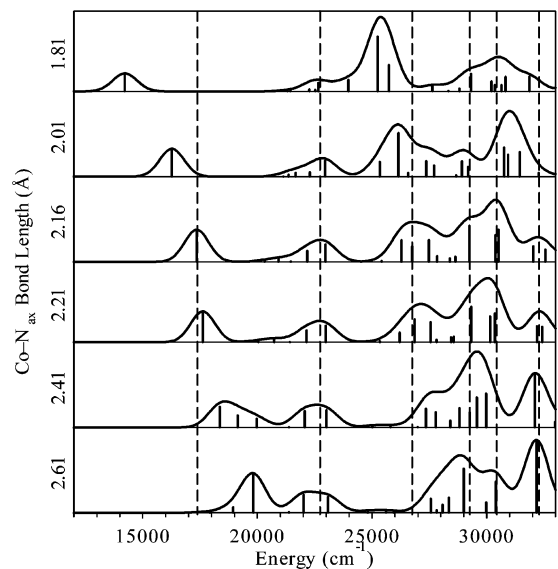
Figure 9. Selected TD-DFT simulated Abs spectra for MeCbl models with fixed lower axial bond lengths between 1.81 and 2.61 Å. Relevant structural parameters for these optimized models are given in Table 2.

function of both coordinates, red-shifting ~ -65 cm^{-1}/pm as the Co−C bond length is increased and blue-shifting ~ 55 cm^{-1}/pm as the Co−N$_{ax}$ bond length is increased. This band shift is due primarily to perturbations of the HOMO that serves as the donor MO in the corresponding transition.[40] As the Co−C bond is lengthened, the HOMO is destabilized due to a weakening of the strong σ-bonding interaction between the Co center and the methyl group that exists in the free MeCbl cofactor (see α/β EDDM in Figure 6). Alternatively, as the Co−N$_{ax}$ bond is stretched, the σ-antibonding interaction between the Co and the imidazole is reduced while the Co−C bonding is largely unaffected, resulting in an overall stabilization of the HOMO. The D/E region of the MeCbl Abs spectrum (Figure 3) is only moderately affected by the alterations in the axial bond lengths, with the band maximum remaining fairly constant even though the contributing transitions are observed to approach one another
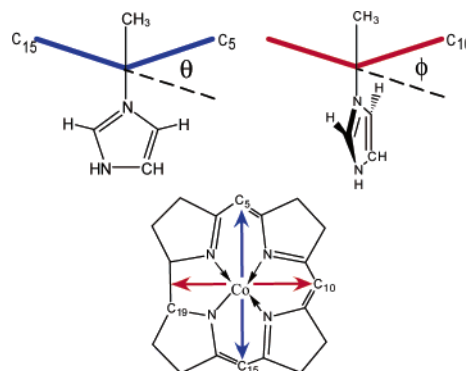
Figure 10. Schematic diagram for folding of the corrin macrocycle. Fold angle θ describes folding along the C^5···C^{15} vector, and fold angle ϕ describes folding along the Co···C^{10} vector.

upon reduction of the bond lengths. Finally, features in the γ-region are affected to varying degrees, with changes of the $\gamma 1$ transition (Figure 6) being most notable.

On the basis of these TD-DFT simulations, it is now possible to correlate spectral shifts observed upon MeCbl-binding to MMCM and generation of the S′ and P′ states with axial ligand deformations under the assumption that structural distortions along other coordinates are negligible. The TD-DFT calculated spectra indicate that the moderate shifts observed in the α/β-region of the MeCbl spectra (bands 1 and 2 in Figure 5B, top) correlate with a ~ 0.03 Å increase in the Co−C bond length or decrease in the Co−N$_{ax}$ bond length upon formation of the R′ state and an opposite bond length change by ~ 0.08 Å upon subsequent binding of substrate to the holoenzyme. While these spectro/structural calculations are thus compatible with both Co−C and Co−N$_{ax}$ bond distortions, a direct modulation of the organometallic bond is unlikely to occur in the protein active site (see Discussion).

(b) Corrin Fold Angles. To explore the effects of macrocycle distortions on the spectral and electronic properties of the MeCbl cofactor, a series of calculations were performed in which the distance between two atoms on opposite sides of the macrocycle was systematically varied (C^5 and C^{15} to vary fold angle θ or C^{10} and C^{19} to vary fold angle ϕ, see Figure 10), with shorter distances leading to an increased fold angle. For our calculations, the C^5···C^{15} distance was varied from 6.351 to 6.651 Å and the C^{10}···C^{19} distance was varied from 5.70 to 6.00 Å, while the remainder of the MeCbl model was subjected to a full geometry optimization. The relevant results from these fold-angle calculations are summarized in Table 3, and the corresponding PESs are shown in Figure 7 (panels C and D).[79]

Focusing first on the fold angle θ, results from the partial DFT geometry optimizations yield valuable insight into the structural and energetic perturbations of the cofactor associated with this mode of distortion. As the fold angle θ increases from 6.28° to 18.56° (corresponding to a decrease in the C^5···C^{15} distance from 6.651 to 6.351 Å), the optimized Co−N$_{ax}$ bond

---

(79) In these fold-angle calculations, the DFT geometry optimizations led to corrin macrocycle conformations that are flatter than observed crystallographically due to the relaxation of steric constraints by modeling the lower axial ligand as an imidazole instead of the full DMB. While a full DFT geometry optimization performed on a model containing the DMB as the lower axial ligand indeed converged to a more folded corrin ($\theta = 9.25°$, $\phi = 9.25°$) for the C^5···C^{15} distance of 6.651 Å, this model was too large to be treated with TD-DFT at the level of theory necessary to produce accurate simulated spectra. Therefore, only the imidazole models are considered in this work.

Table 3. Results from Partial DFT Geometry Optimizations for the MeCbl Model in Which the Distance between Two C Atoms on Opposite Sides of the Macrocycle Was Fixed and the Energy Was Minimized with Respect to All Other Atomic Coordinates[a]

$r(C^5 \cdots C^{15})$ (Å)	fold angle θ (deg)	Co–C (Å)	Co–N_{ax} (Å)	relative E (kcal/mol)
6.351	18.56	1.999	2.196	4.663
6.451	13.59	1.996	2.210	2.110
6.551	7.69	1.996	2.209	0.465
6.651	6.28	1.997	2.206	0.000

$r(C^{10} \cdots C^{19})$ (Å)	fold angle ϕ (deg)	Co–C (Å)	Co–N_{ax} (Å)	relative E (kcal/mol)
5.70	15.63	2.01	2.178	6.878
5.80	10.26	2.002	2.197	3.759
5.90	3.62	1.999	2.203	1.382
6.00	2.56	1.996	2.210	0.000

[a] Experimental structure values: MeCbl,[77] $r(C^5 \cdots C^{15})$ = 6.651 Å, θ = 14.76°, $r(C^{10} \cdots C^{19})$ = 6.001 Å, ϕ = 12.84°, $r(Co-C)$ = 1.979, $r(Co-N_{ax})$ = 2.163 Å; AdoCbl,[30] $r(C^5 \cdots C^{15})$ = 6.680 Å, θ = 13.34, $r(C^{10} \cdots C^{19})$ = 6.056 Å, ϕ = 13.09°, $r(Co-C)$ = 2.030, $r(Co-N_{ax})$ = 2.203 Å.
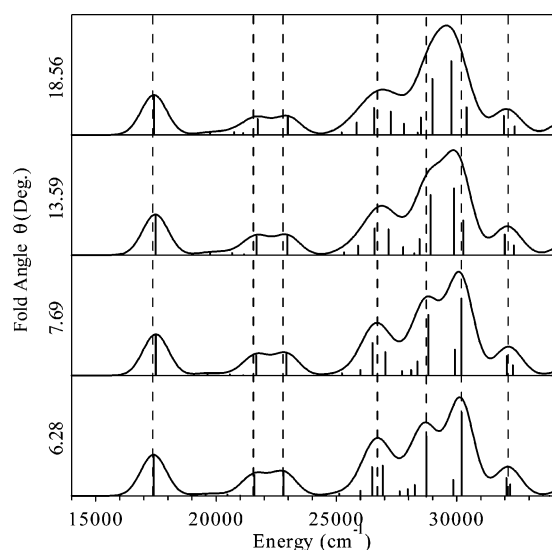
Figure 11. TD-DFT simulated Abs spectra for MeCbl models differing with respect to their fold angle θ. Relevant structural parameters for these optimized models are given in Table 3.

distance decreases by 0.015 Å (Table 3). Even with this significant change in the fold angle and small upward motion of the lower histidine ligand, only negligible changes are observed for the Co–C bond distance (a total of 0.002 Å). Interestingly, the energies for the converged structures described in Table 3 are extremely similar, varying by only 4.7 kcal/mol over the ∼12° surveyed. Consequently, the resultant PES is extremely flat for this folding motion (Figure 7C), suggesting that it is energetically feasible for such distortions to occur in the protein active site.

The TD-DFT calculated Abs spectra for the various MeCbl models differing with respect to θ (Table 3) are shown in Figure 11. Contrary to the axial ligand perturbations, an increase in the fold angle θ by as much as ∼20° has almost no effect on the α/β transition, which red-shifts by only -7 cm^{-1}/deg because the HOMO/LUMO gap remains largely unperturbed for distortions along this coordinate. Small changes are observed in the D/E and γ regions, however, with band shifts and intensity redistributions being most prominent for the $\gamma 2$ and $\gamma 3$ transitions that approach one another as the corrin macrocycle folding increases. The $\gamma 2$ transition involves a corrin π^*-based acceptor MO that possesses a significant σ-antibonding contri-
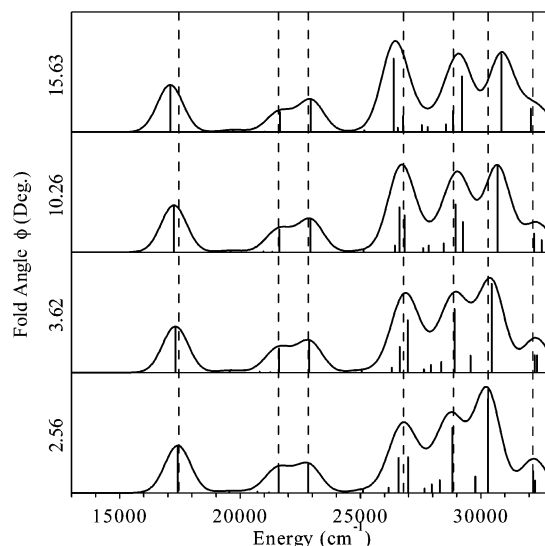
Figure 12. TD-DFT simulated Abs spectra for MeCbl models differing with respect to the fold angle ϕ. Relevant structural parameters for these optimized models are given in Table 3.

bution from the Co 3d$_{x^2-y^2}$ orbital. As the fold angle of the corrin macrocycle increases, this Co 3d$_{x^2-y^2}$ orbital contribution increases, leading to an overall destabilization of the corresponding MO and thus to a blue-shift of the $\gamma 2$ band by 20 cm^{-1}/deg. At the same time, this increase in the fold angle θ causes the $\gamma 3$ band to red-shift by -35 cm^{-1}/deg.

Turning now to the fold angle ϕ, the results from partial DFT geometry optimizations with fixed $C^{10} \cdots C^{19}$ distances reveal larger variations in the Co–C and Co–N_{ax} bond lengths as compared to folding along θ (Table 3). As ϕ increases from 2.56° to 15.63°, the Co–C bond lengthens by 0.015 Å and the Co–N_{ax} bond shortens by almost 0.04 Å. Nevertheless, these folding-induced perturbations of the axial bond lengths are still considerably smaller than those associated with modulations of the trans axial bond lengths (cf. Tables 2 and 3). The energy range that these geometries sample is comparable to that found for variations in the fold angle θ, again leading to a fairly flat PES (Figure 7D), with the lowest energy structure corresponding to the model with the smallest fold angle.

The results from TD-DFT calculations on the $C^{10} \cdots C^{19}$ constrained structures are shown in Figure 12. As for variations in θ, the α/β transition also shows minimal shifts with increasing fold angle ϕ (30 cm^{-1}/deg), signifying that alterations in the HOMO/LUMO gap energies are again negligible. Likewise, both the position and the intensity of the $\gamma 1$ transition remain fairly constant for this mode of distortion. Contrastingly, the $\gamma 2$ and $\gamma 3$ transitions are predicted to be perturbed substantially, blue-shifting by ∼34 and 50 cm^{-1}/deg, respectively, as the fold angle increases.

Following the same approach as outlined above for the axial ligand perturbations, the TD-DFT calculated spectra for the various fold angles can now be used to determine the maximum degree of macrocycle folding possible based on the experimental band shifts observed, this time assuming that distortions involving the axial ligands are negligible. The red-shift of the $\gamma 2$ band observed in the experimental spectrum (Figure 6) upon MeCbl binding to MMCM corresponds to a maximum 20° decrease in the fold angle θ or 12° decrease in the fold angle ϕ. Upon substrate analogue binding to holo-MMCM, our

spectro/structural correlations reveal a maximum fold angle change by 17° based on the 600 cm^{-1} blue-shift of the $\gamma 3$ band, corresponding to a flattening of the macrocycle along θ or an increase in the fold angle ϕ. Neither set of fold angle calculations can account for the experimental shifts of the α/β bands, however, indicating that sizable distortions must also occur along coordinates other than the macrocycle fold angle.

4. Discussion

Despite many years of dedicated research, the mechanism by which B$_{12}$-dependent enzymes achieve the tremendous rate enhancement for the catalytically essential Co−C bond cleavage step (Figure 2) has remained poorly understood. Building upon the foundation of our recent studies on free Co^{3+}corrinoids,[40] the quantitative analysis of Abs and MCD spectroscopic data of MMCM-bound AdoCbl and MeCbl within the framework of our DFT/TD-DFT generated spectro/structural correlations developed in this work provides significant new insight into the cofactor/enzyme interactions in the Co^{3+}Cbl "ground" state. Discussed below are key findings from this research and their possible implications with respect to enzymatic Co−C bond activation mechanisms proposed in the literature.

Cofactor Binding to apo-MMCM. Dependence of Cofactor/MMCM Interactions on the Upper Axial Ligand. To explore the dependence of the Co^{3+}Cbl/MMCM interactions on the identity of the cofactor's upper axial ligand, Abs and MCD spectra of the resting state were obtained using the native cofactor AdoCbl (R state, Figure 2) and its derivative MeCbl (R' state). The similarities in the electronic spectra of free and MMCM-bound AdoCbl (Figure 3, top) suggest that only minimal perturbations of the geometric and electronic structures of the cofactor are induced by the protein active site in the R state. The band sharpening observed in these spectra suggests that the AdoCbl cofactor adopts a well-defined conformation when it binds to MMCM, possibly through stabilization of one of the several roughly isoenergetic orientations of the Ado moiety that exist in solution.[66,67] This is an important result, as crystal structures have frequently failed to provide information on the location of the Ado moiety in the active site due to facile X-ray photoreduction of the cofactor in the X-ray beam.[22]

In comparison to AdoCbl, the sterically less constrained MeCbl cofactor appears to undergo more significant changes upon binding to MMCM to generate the R' state, as evidenced by the larger alterations of the Abs and MCD spectra for this species (Figure 3, bottom). As such, it appears that the bulky Ado moiety may restrict geometric changes in the AdoCbl structure that otherwise (e.g., in the case of MeCbl) would occur through steric strain imposed by the protein active site. Therefore, the less sterically hindered MeCbl cofactor offers a superior probe of the cofactor/MMCM interactions in the Co^{3+}-Cbl "ground" state. Based on the spectro/structural correlations developed in the Computational section above, a bond length change of ~0.03 Å for either axial ligand (+0.03 for the Co−C bond or −0.03 for the Co−N$_{ax}$ bond) could explain the experimental shifts of the α/β bands upon formation of the R' state. While corrin ring deformations could in principle also contribute to the observed shifts of the α/β bands, our TD-DFT calculated Abs spectra (Figures 8, 9, 11, and 12) indicate that only the axial ligand perturbations give rise to significant changes to the α/β-region. This great sensitivity of the α/β band

positions on axial ligand perturbations stems from the fact that the energy of the donor orbital in the corresponding transition (i.e., the HOMO) is finely tuned by the extent of Co−C σ-bonding and Co−N$_{ax}$ σ-antibonding contributions to this MO (see α/β EDDM, Figure 6). Consequently, a most convenient probe of Co−N$_{ax}$ axial ligand distortions in any B$_{12}$-dependent enzyme involves estimating band shifts in the α,β-region of the Abs spectrum upon cofactor binding to the active site and comparing the values obtained to the plot in Figure 10.

Effects of Lower Axial Ligand Switch. It has been known for almost a decade that MMCM is a member of the "base-off" class of Cbl-dependent enzymes in which the intramolecular DMB coordinating in the lower axial position of the free cofactor is replaced by a histidine from the enzyme active site (His^{610} in the case of MMCM).[29] These results surprised many upon their discovery, and it was thought that this ligand switch might play an important role in activating the Co−C bond for homolysis. While an unusually long axial Co−N$_{ax}$ bond length of 2.53 Å was originally observed crystallographically by Mancia et al.[28] for AdoCbl bound to MMCM (R state, Figure 2), subsequent EXAFS spectroscopic studies[24,31,32] yielded inconclusive results, consistent with a Co−N$_{ax}$ bond length of either ~2.2 or ~2.5 Å.

Our spectro/structural correlations developed in this study now allow for a straightforward evaluation of this proposal of an unusually long Co−N$_{ax}$ bond based on the changes observed in the experimental spectra upon cofactor binding to MMCM. The most direct probe of axial ligand distortions is provided by the α/β bands, as the energies of these bands remain essentially unchanged upon corrin ring deformations (Figures 11 and 12). Importantly, the observed red-shift by ~ −170 cm^{-1} of the α/β bands associated with MeCbl binding to apo-MMCM (Figure 5B) reveals that, if anything, the Co−N$_{ax}$ bond actually shortens by ≤0.03 Å (Figure 9). A small Co−N$_{ax}$ bond shortening upon cofactor binding to MMCM is not unexpected, as the imidazole side chain of His^{610} can more easily approach the corrin macrocycle than the bulkier DMB ligand. From Figure 9, a ~0.3 Å Co−N$_{ax}$ bond length increase as proposed earlier would result in a dramatic blue-shift of the α/β bands by ~1650 cm^{-1} rather than the observed red-shift. This prediction concurs nicely with experimental Abs data of free MeCbl and AdoCbl; that is, substitution of the DMB ligand that binds to the Co center at neutral pH (a strong σ-donor) by a water molecule at low pH (a weak donor and thus a reasonable model of a His ligand separated by ~2.5 Å from the Co center) gives rise to a large blue-shift of the α/β bands by ~2000 cm^{-1}.[40] Note that the TD-DFT computed shift of ~2500 cm^{-1} almost quantitatively reproduces this experimental finding,[40] lending further credence to our spectroscopic/computational methodology employed here.

Our calculations reveal further that increasing the Co−N$_{ax}$ bond length to 2.51 Å, while quite unlikely based on energetic considerations alone (Figure 7B), also fails to affect the Co−C bond properties to any significant degree (Table 2). On the basis of these results, we conclude that the long Co−N$_{ax}$ bond observed by X-ray crystallography presumably results from redox heterogeneity of the cofactor in the enzyme active site. Thus, our data together with the RR results of Banerjee, Spiro, and co-workers,[20] which indicated a maximum reduction in the Co−C bond dissociation energy by 0.5 kcal/mol upon formation

of the R state, provide convincing evidence against any significant weakening of the Co–C bond induced by the DMB → His ligand switch accompanying cofactor binding to MMCM.

Substrate/Product Binding to holo-MMCM. By using the three different substrate and product (analogues) in Charts 1 and 2, we were able to investigate the S/S′ and P/P′ states for MMCM reconstituted with AdoCbl and MeCbl (Figure 2). Akin to the results for the R state, the spectroscopic data for the S and P states reveal only minor changes relative to the free AdoCbl spectra (confined to small shifts of bands 3, 4, and 9, Figure 5). In comparison, the S′ and P′ spectra differ quite substantially from those obtained for the R′ state and, to a lesser degree, for free MeCbl. As the MeCbl cofactor demonstrates increased flexibility over AdoCbl, it is tempting to speculate that the former is better suited to adopt a conformation closer to that preferred by the $Co^{2+}Cbl$ "intermediate" state (I state, Figure 2). On the basis of our spectro/structural correlations, the 450 cm^{-1} blue-shift of band 1 in the S′ and P′ state spectra with respect to the R′ state spectra of MMCM-bound MeCbl (Figure 4, bottom) corresponds to an elongation of the Co–N_{ax} bond by 0.08 Å or shortening of the Co–C bond by 0.07 Å (note that corrin ring deformations do not contribute markedly to shifts of band 1, see Figures 11 and 12). As a compression of the Co–C bond length can be ruled out on the basis of energetic grounds (Figure 7) and steric considerations (i.e., as the MMCM active site has evolved to accommodate the bulkier AdoCbl cofactor, it is not expected that the methyl group of enzyme-bound MeCbl interacts with amino acid side chains), it is reasonable to ascribe this spectral shift to an elongation of the lower axial Co–N_{ax} bond by ≤0.08 Å upon addition of substrate/product (analogues) to holo-MMCM. This predicted lengthening is still minor as compared to the crystallographically observed elongation of the Co–N_{ax} bond in holo-MMCM,[28] however, and does not contradict our assertion that the "hyper-long" bond is an artifact of the redox heterogeneity caused by X-ray photoreduction. Moreover, our results indicate that the crystallographically observed change in protein conformation upon substrate binding to holo-MMCM[22] most likely occurs concomitant with or following Co–C bond homolysis, possibly aiding in stabilization of the $Co^{2+}Cbl$ intermediate (I state, Figure 2).

Implications for Co–C Bond Activation Mechanism. Throughout the entire history of enzymatic B_{12} research, investigators have proposed theories as to how AdoCbl-dependent enzymes utilize the resources at their disposal to activate the cofactor's Co–C bond for homolysis. In the following, some of the most popular bond activation mechanisms proposed in the literature are evaluated on the basis of the spectroscopic and computational results presented above.

Inverse Trans Effect. The basis for the inverse trans effect theory is an electronic perturbation of the Co–C bond via the lower axial ligand. In traditional organometallic chemistry, the trans effect is a direct relationship between two trans ligands, stating that when one ligand forms a stronger bond with the metal center, electron density is removed from the bond to the trans ligand, weakening the interaction of the trans ligand with the metal.[80] From an analysis of crystallographic data for many cobalamin and cobaloxime species, De Ridder et al.[81] found

that, contrary to the normal behavior, the trans Co–C and Co–N_{ax} bond distances are positively correlated, resulting in an inverse trans effect. With the crystallographic observation of an unusually long Co–N_{ax} bond length for MMCM,[28] it was proposed that an inverse trans effect may be operative, where a protein-induced lengthening of the Co–N_{ax} bond would trigger a weakening of the trans Co–C bond. However, this theory is flawed in two respects based on results from our research as well as published RR[75] and EXAFS[31,32] data. First, the existence of an unusually long Co–N_{ax} bond itself is questionable, with most current results, in particular our spectro/structural correlations presented herein, indicating that this observation most likely reflects redox heterogeneity of the cofactor in the X-ray structures. Second, even if the Co–N_{ax} bond were longer in the enzyme active site than in the free cofactor, our calculations do not indicate any significant weakening of the trans Co–C bond as a function of the Co–N_{ax} bond distance (Table 2). This result is consistent with published RR data and IR vibrational data for alkyl-$Co^{3+}Cbls$, which demonstrated that changing the identity of the lower axial ligand has negligible effects on the Co–C bond strength.[75,82–84] Together with the RR results from Banerjee, Spiro et al., which revealed a weakening of the Co–C bond by merely 0.5 kcal/mol upon AdoCbl binding to MMCM,[20] our data indicate that the inverse trans effect is not likely to play an important role in the $Co^{3+}Cbl$ ground-state activation mechanism. It is interesting to note, however, that the reported Co–N_{ax} bond length of 2.5 Å is also unusually long for the reduced form of the cofactor and, as such, this unusual structural feature may actually be of relevance to the enzymatic stabilization of the $Co^{2+}Cbl$ intermediate state.

Co–C Bond Tilting (Tyr89 Wedge). A straightforward mechanism for weakening of the Co–C bond in the ground state would involve direct interaction of the Ado moiety with the protein active site, leading, for example, to Co–C bond tilting. Such a proposal was originally formulated by Banerjee, Spiro, and co-workers[20] based on RR studies that revealed an intensity transfer from the Co–C stretching mode to the Co–C–C bending mode upon AdoCbl binding to the enzyme active site. In support of this proposal, an active site residue (Tyr89) has been identified that is properly positioned to interact strongly with the Ado moiety. In crystal structures of substrate analogue bound holo-MMCM, this Tyr89 residue is located in a position thought to be initially occupied by the Ado moiety.[22] Moreover, mutagenesis of Tyr89 to Phe resulted in loss of catalytic activity of MMCM, confirming that Tyr89 is poised to play an important role in the catalytic Co–C bond activation mechanism.[85] As our spectroscopic probes are not directly sensitive to changes in the Co–C–C bond angle, we do not observe any spectral differences between the S and P states that would indicate the occurrence of Co–C bond tilting in the S state and subsequent straightening upon formation of the P state. However, provided that such enzymatic modulations in Co–C–C bond angle do indeed occur, our results indicate that their effect on the Co–C bond length and, thus, the bond strength must be minor, as the

(80) Spessard, G. O.; Miessler, G. L. *Organometallic Chemistry*; Prentice Hall: New Jersey, 1997.

(81) De Ridder, D. J. A.; Zangrando, E.; Bürgi, H. B. *J. Mol. Struct.* **1996**, *374*, 63–83.
(82) Puckett, J. M.; Mitchell, M. B.; Hirota, S.; Marzilli, L. G. *Inorg. Chem.* **1996**, *35*, 4656–4662.
(83) Dong, S. L.; Padmakumar, R.; Banerjee, R.; Spiro, T. G. *J. Am. Chem. Soc.* **1996**, *118*, 9182–9183.
(84) Taraszka, K. S.; Chen, E.; Metzger, T.; Chance, M. R. *Biochemistry* **1991**, *30*, 1222–1227.
(85) Vlasie, M. D.; Banerjee, R. *J. Am. Chem. Soc.* **2003**, *125*, 5431–5435.

α/β bands remain in the same position for the R, S, and P states. Our data thus fill an important gap in the current understanding of enzymatic Co−C bond activation, as RR experiments failed to explore how ν_{Co-C} is affected by substrate and product binding to holo-MMCM.[20]

Macrocycle Folding. The increased flexibility of the corrin ring over the porphyrin macrocycle due to the more reduced nature of the former has been invoked to play a key role in the enzymatic destabilization of the Co−C bond.[86,87] By carrying out a butterfly-like bending motion, the corrin macrocycle could potentially exert pressure on the bulky Ado moiety, thereby weakening the upper axial Co−C bond. However, numerous experimental studies have provided evidence against this mechanochemical triggering scheme. For example, X-ray crystallographic data suggest that the macrocycle actually achieves a flatter conformation in the enzyme active site than in solution.[28] Also, RR studies on holo-MMCM revealed that the frequencies of corrin breathing modes do not change upon conversion of the R state to either the S or the P states,[20] arguing against substrate- or product-induced modulations of the macrocycle folding.

Nonetheless, RR frequency upshifts of the corrin modes were observed upon AdoCbl-binding to apo-MMCM, which were tentatively ascribed to a flattening of the macrocycle on the basis of a comparison with RR data of heme systems.[88] However, as the corrin macrocycle is inherently more complex than the porphyrin ring, such a comparison is not necessarily valid. Indeed, it is interesting to note that, while the fold angle θ increases by 5.4° from AdoCbl to H_2OCbl^+, both the short-axis (ν_{SA}) and the long-axis (ν_{LA}) corrin modes shift to higher frequencies by ∼3 and 6 cm^{-1}, respectively.[40] Although electronic factors associated with this upper axial ligand substitution presumably also affect the frequencies of corrin-based modes, ν_{SA} and ν_{LA} decrease by 6 and 1 cm^{-1} from AdoCbl to Ado-cobinamide (which lacks the DMB moiety and instead binds a water molecule in the lower axial position) despite the expected flattening of the macrocycle and the decrease in donor strength of the lower axial ligand (thus reducing the extent of $Co^{3+} \rightarrow \pi^*$ charge donation).[40] Collectively, these experimental results suggest that, contrary to the correlation established for heme systems,[88] the corrin-based modes actually shift to higher energy as the macrocycle folding increases. In support of this model, our preliminary DFT frequency calculations for MeCbl predict frequency upshifts of corrin-based normal modes as θ is increased from 18° to 25° (Figure S4).

Regardless of the exact nature of the corrin ring deformations induced by the protein active site, the fact that our Abs and MCD spectra for free and MMCM-bound AdoCbl are nearly identical (Figure 3, top) demonstrates that these distortions must be minor. Consistent with the more flexible nature of MeCbl as compared to that of AdoCbl, the corresponding Abs and MCD spectra exhibit more dramatic changes upon cofactor binding to MMCM. On the basis of the spectro/structural correlations developed herein (Figures 8, 9, 11, and 12), these changes can be interpreted in terms of a Co−N_{ax} bond shortening by 0.03 Å coupled to an increase in θ by ∼8°. Thus, while the enzyme may indeed slightly enhance macrocycle folding in the Co^{3+}-Cbl ground state, the fact that the Co−C bond properties for both AdoCbl and MeCbl remain largely unperturbed upon cofactor binding to apo-MMCM suggests that modulations of the corrin ring conformation might be important primarily with respect to the enzymatic stabilization of the $Co^{2+}Cbl$ intermediate state.

5. Conclusions

By developing a combined spectroscopic/computational methodology, we have been able to probe the nature of the interactions between AdoCbl (and MeCbl) and the MMCM active site in the R (R′), S (S′), and P (P′) states and to assess the importance of these interactions with respect to the enzymatic Co−C bond activation mechanism. While the spectra of AdoCbl display only minor changes upon cofactor binding to MMCM and subsequent addition of substrate analogues to the holoenzyme, the use of the sterically less constrained cofactor analogue MeCbl has permitted unique insight into the structural distortions imposed on the cofactor as the enzyme progresses through the reaction cycle. Together, our spectroscopic and computational results indicate that, although the enzyme perturbs the cofactor in its $Co^{3+}Cbl$ ground state to a small degree, the dominant contribution to the enzymatic Co−C bond activation presumably comes through stabilization of the $Co^{2+}Cbl/Ado^{\bullet}$ post-homolysis products. Spectroscopic and computational studies on free and MMCM-bound $Co^{2+}Cbl$ are currently underway in our laboratory to evaluate this proposal.

Supporting Information Available: Abs and MCD spectra for the P state (GCoA) and the S′ state (MMCoA), all Gaussian deconvolutions not shown in the text, simulated MeCbl Raman spectra, and Cartesian coordinates for all computational models. This material is available free of charge via the Internet at http://pubs.acs.org.

JA039114B

(86) Glusker, J. P. In *B₁₂*; Dolphin, D., Ed.; Wiley: New York, 1982; Vol. 1, pp 23−106.
(87) Geno, M. K.; Halpern, J. *J. Am. Chem. Soc.* **1987**, *109*, 1238−1240.
(88) Spiro, T. G. *Biological Applications of Raman Spectroscopy*; Wiley: New York, 1987.